Journal of Organometallic Chemistry 694 (2009) 3781–3792

Contents lists available at ScienceDirect

Journal of Organometallic Chemistry

journal homepage: www.elsevier.com/locate/jorganchem

Experimental and theoretical characterization of Ru(II) complexes with polypyridine and phosphine ligands

Mauricio Yáñez [a], Juan Guerrero [b], Pedro Aguirre [c], Sergio A. Moya [d,*], Gloria Cárdenas-Jirón [e,*]

[a] Laboratorio de Recursos Renovables, Centro de Biotecnología, Universidad de Concepción, Concepción, Casilla 160-C, Chile
[b] Laboratorio de Resonancia Magnética Nuclear, Facultad de Química y Biología, Universidad de Santiago de Chile, Chile
[c] Facultad de Ciencias Químicas y Farmacológicas, Universidad de Chile, Chile
[d] Laboratorio de Química Organometálica y Catálisis, Facultad de Química y Biología, Universidad de Santiago de Chile, Chile
[e] Laboratorio de Química Teórica, Facultad de Química y Biología, Universidad de Santiago de Chile (USACH), Casilla 40, Correo 33, Santiago, Chile

ARTICLE INFO

Article history:
Received 26 January 2009
Received in revised form 13 July 2009
Accepted 14 July 2009
Available online 17 July 2009

Keywords:
Ruthenium
Polypyridine
Phosphine
Electronic absorption spectra
TD-DFT

ABSTRACT

The synthesis and the experimental and theoretical characterization of ruthenium hydride complexes containing phosphorus and polypyridine ligands $[RuH(CO)(N\text{-}N)(PPh_3)_2]^+$ with N-N = dppz **1**, dppz-CH_3 **2** (**2.1** isomer), dppz-Cl **3** (**3.1** isomer), ppl **4,** and 2,2′-biquinoline **5**, (where dppz = dipyrido[3,2-a:2′,3′-c]phenazine), are presented. ^1H NMR, ^{31}P NMR, ^{13}C NMR, IR-FT, UV–Vis and elemental analysis are used to characterize the complexes. Optimized molecular geometries in the gas phase at the B3LYP/LACVP(d,p) level showed a distorted octahedral structure for ruthenium, the phosphine ligands are localized in a *trans* position, while the polypyridine ligand, which in all the cases is planar except in **5**, adopt a *trans* position relative to the carbon monoxide and hydride ligands. The theoretical absorption spectra (one hundred excited states) were calculated for the seven complexes by the time dependent density functional theory (TD-DFT) in the gas phase. They predicted very well the UV–Vis spectra. It was possible to identify the character of each electronic transition and the fragments of the complexes involved in it. Theoretical evidence of the substituent effect in the polypyridine ligand and of the ligand effect (dppz, biq, ppl) was found, displayed mainly in the longer wavelength band. The theoretical results showed that the properties of these complexes can be tuned with changes localized in the polypyridine ligand covalently bonded to ruthenium.

1. Introduction

Hydrides of the transition metals Fe, Co, Ni, Ru, Rh and Pd have been applied as catalysts in numerous reactions presenting high activity and selectivity [1]. Of these complexes, ruthenium hydride containing carbonyl and triarylphosphine ligands have attracted enough attention due to their reactivity and efficiency as catalysts in hydrogenation reactions of unsaturated substrates, hydrogen transfer, activation of C–H bonds, and isomerization reactions [2–9].

On the other hand, complexes of ruthenium containing π-acceptor nitrogen-bearing ligands such as polypyridines have been widely studied as systems for the conversion of solar energy in storable energy [10]. However, the study and application of ruthenium hydride containing triphenylphospine and polypyridine ligands simultaneously in the coordination sphere has been limited to a few specific examples [11].

Here we report an experimental and quantum chemical study of ruthenium complexes of the type $[RuH(CO)(N\text{-}N)(PPh_3)_2]^+$, where N-N = 2,2′-biquinoline (biq), dipyrido[3,2-a:2′,3′-c]phenazine (dppz-R, with R = H, Me, Cl), and pyrazine[2,3-f][1,10]-phenanthroline (ppl). The quantum chemical study included a characterization of the molecular and electronic structures of the complexes by analysis of optimized molecular geometries and electronic populations by using the natural bond orbitals (NBO) scheme. The latter was used to identify the nature of the interactions between the ligands and the central metal atom. The quantum methodology called time dependent density functional theory (TD-DFT) [12–14] was finally used to calculate the electronic absorption spectra. Based on a molecular orbital scheme, these results allowed the interpretation of the UV–Vis spectra obtained at an experimental level.

2. Experimental

2.1. Materials

The chemicals used for the synthesis of the ligands, complexes, and deuterated solvents were obtained from Sigma–Aldrich. The phosphines used were purchased from Strem. All solvents used were analytical grade from J.T. Baker. Solvents were dried accord-

* Corresponding author.
E-mail addresses: mayanez@udec.cl (M. Yáñez), sergio.moya@usach.cl (S.A. Moya), gloria.cardenas@usach.cl (G. Cárdenas-Jirón).

0022-328X/$ - see front matter © 2009 Elsevier B.V. All rights reserved.
doi:10.1016/j.jorganchem.2009.07.028

ing to published procedures [15a], and were distilled before use. Complex polypyridine ligands were prepared following reported procedure. Simple nitrogenous ligands such as 2,2-biquinoline were purchased from Sigma–Aldrich. Dppz and replaced dppz were prepared using reported procedures. [15b].

1D ^{1}H NMR, ^{31}P{^{1}H} NMR, ^{13}C{^{1}H} NMR, and 2D-ge ^{1}H ^{1}H COSY, 2D ^{1}H ^{13}C HSQC-ed, and 2D ^{1}H ^{13}C HMBC NMR spectra were recorded on a Bruker Avance 400 MHz spectrometer (400.133 MHz for ^{1}H, 100.624 MHz for ^{13}C, 161.976 MHz for ^{31}P) equipped with a 5 mm broad band inverse probe head gradient enhanced. All the measurements were made at 300 K and chemical shifts (δ in ppm) for ^{1}H, ^{13}C were reported relative to Me_4S, and for ^{31}P relative to 85% H_3PO_4.

IR spectra were obtained on a Bruker IFS-66 V FT-IR spectrophotometer with solid samples in 0.22-mm thick KBr disks. Elemental analysis was carried out using a CE Instruments EA 1108 model.

Electronic spectra were obtained on a UV–Vis SPECORD S 100 spectrophotometer. Melting points of the compounds was determined on an Electrothermal 9100 apparatus.

2.2. Synthesis and characterization of ruthenium complexes of type [RuH(CO)(NN)(PPh$_3$)$_2$]PF$_6$]

The compounds used in this study (Fig. 1) were prepared using the following general experimental procedure, varying in each case the corresponding NN ligand.

The precursor, RuHCl(CO)(PR$_3$)$_3$ and the ligand NN [N-N:PR$_3$ = (**1**) dppz:PPh$_3$ (**2**) dppz-CH$_3$:PPh$_3$ (**3**) dppz-Cl:PPh$_3$ (**4**) ppl:PPh$_3$ (**5**) 2,2-biq:PPh$_3$ dissolved in ethanol were refluxed for three hours. The solution was cooled to room temperature, the volume was reduced to one third, and ammonium hexafluorophosphate in ethanol was added to produce a precipitate. The solid was separated by filtration, washed with two volumes of hexane, recrystallized from diethylether, and dried under vacuum.

2.3. [RuH(CO)(dppz)(PPh$_3$)$_2$]PF$_6$ (*1*)

Colour: light brown. ^{1}H NMR (CD_3COCD_3): δ 9.57 (H_a, d, $^3J_{ab}$ = 8.9), 9.47 (H_{a1}, d, $^3J_{a1b1}$ = 8.9), 7.96 (H_b, dd, $^3J_{bc}$ = 5.1), 7.2–7.4 (H_{b1}) (overlapping the triphenylphosphine signals), 9.70 (H_c, d, $^3J_{cb}$ = 5.1), 8.37(Hc_1, d, $^3J_{c1b1}$ = 5.1), 8.46 (H_d + H_{d1}, m), 8.17 (H_e + H_{e1}, m); −10.99 (hydride, t, J_{HP} = 19.83); ^{31}P NMR: 46.50, IR (KBr pellets, cm^{-1}): ν (Ru–H) = not observed; ν (CO) = 1937 (*vs*); ν (C=C, C=N) = 1436–1480 (*m*); ν (PF_6^-) = 839 (*vs*). Melting point 330 °C (d). Yield 70.4%. Elem. Anal. Calc. for $C_{55}H_{41}F_6N_4OP_3Ru$: C, 61.05; H, 3.81; N, 5.17. Found: C, 61.7; H, 3.87; N, 5.43%.

2.4. [RuH(CO)(dppz-CH$_3$)(PPh$_3$)$_2$]PF$_6$ (*2* and *2.1*)

Colour: light brown. ^{1}H NMR: (CD_3COCD_3), δ 8.34 (H_a, m), 8.34 (H_{a1}, m), 7.98 (H_b, m), 7.98 (H_{b1}, m), 9.54 (H_c, d), 9.44 (H_{c1},d), 8.23 (H_d, d), 9.69 (H_{d1}, s), 7.4–7.2 (H_e) (overlapping the triphenylphosphine signals), 2.8 (CH_3), −10.99 (hydride, t, J_{HP} = 19.21). ^{31}P NMR: 46.48. IR (KBr, cm^{-1}): ν (Ru–H) = 2014 (*m*); ν (CO) = 1934 (*vs*); ν (C=C, C=N) = 1435–1481 (*m*); ν (PF_6^-) = 841 (*vs*). Yield: 85.5%. Elem. Anal. Calc. for $C_{56}H_{43}F_6N_4OP_3Ru$: C, 61.37; H, 3.95; N, 5.11. Found: C, 59.99; H, 3.92; N, 5.07%.

2.5. [RuH(CO)(dppz-Cl)(PPh$_3$)$_2$]PF$_6$ (*3* and *3.1*)

Colour: brown. ^{1}H NMR: (CD_3COCD_3), δ 8.49 (H_a, m), 8.49 (H_{a1}, m), 7.98 (H_b, m), 7.4–7.2 (H_{b1}) (overlapped by the triphenylphosphine signals), 9.53 (H_c, d, $^3J_{cb}$ = 7.68), 9.44 (H_{c1}, d, $^3J_{c1b1}$ = 7.68), 8.37 (H_d, s), 9.74 (H_{d1},s), 8.14 (H_e, d); −11.01 (hydride, t, J_{HP} = 19.21), ^{31}P NMR: 46.44, IR (KBr, cm^{-1}): ν (Ru–H) = 2009 (*m*); ν (CO) = 1934 (*vs*); ν (C=C, C=N) = 1433–1487 (*m*); ν (PF_6^-) = 839 (*vs*); ν (C–Cl) = 1091 (*m*). Yield 88%. Elem. Anal. Calc. for $C_{55}H_{40}ClF_6N_4OP_3Ru$: C, 59.17; H, 3.61; N, 5.01. Found: C, 58.99; H, 3.49; N, 4.98%.

2.6. [RuH(CO)(ppl)(PPh$_3$)$_2$]PF$_6$ (*4*)

Colour: yellow. ^{1}H NMR: δ 9.63 (H_a, d, $^3J_{ab}$ = 7.68), 9.53 (H_{a1}, d, $^3J_{a1b1}$ = 8.23), (7.5–7.3) (overlapped by the protons of the triphenylphosphine) (H_b), 8.16 (H_{b1}, q, $^3J_{b1a1}$ = 8.23), 9.92 (H_c, d, $^3J_{cb}$ = 5.48), 8.6 (H_{c1}, d, $^3J_{c1b1}$ = 5.48), 9.42 (H_d + H_{d1}, m); −11.25 (hydride, t, J_{HP} = 18.88). ^{31}P NMR: 43.90. IR (KBr, cm^{-1}): ν (Ru–H) = Not observed; ν (CO) = 1948 (*vs*); ν (C=C, C=N) = 1435–1481 (*m*); ν (PF_6^-) = 837 (*vs*). Yield 89%. Elem. Anal. Calc. for $C_{51}H_{39}F_6N_4OP_3Ru$: C, 59.36; H, 3.81; N, 5.93. Found: C, 58.90, H, 3.60; N, 5.45%.

2.7. [RuH(CO)(biq)(PPh$_3$)$_2$]PF$_6$ (*5*)

Colour:yellow-orange. ^{1}H NMR: δ 9.06 (H_a, s), 8.24 (H_{a1}, d), 8.4 (H_b, m), 7.35 (H_{b1}, m), 7.59 (H_c, t), 7.35 (Hc_1, m), 8.09 (H_d, d) 7.84 (H_{d1}, d), 8.4 (H_e, m), 7.35 (H_{e1}, m), 8.4 (H_f, m), 7.35 (H_{f1}, m); −11.03 (hydride, t, J_{HP} = 18.55). ^{31}P NMR: 43.77. IR (KBr, cm^{-1}): ν (Ru–H) = Not observed; ν (CO) = 1940 (*vs*); ν (C=C, C=N) = 1434–1509 (*m*); ν (PF_6^-) = 839 (*vs*). Yield 86%. Elem. Anal. Calc. for $C_{55}H_{43}F_6N_2OP_3Ru$: C, 62.56; H, 4.10; N, 2.65. Found: C, 61.80; H, 3.95; N, 2.50%.

3. Computational methods

Molecular geometries of the singlet ground state of complexes **1**–**5** of the series [RuH(CO)(N-N)(PPh$_3$)$_2$]$^+$ (Fig. 1) were fully optimized in the gas phase at the B3LYP/LACVP(d,p) level of theory using the Jaguar 6.0 package [16]. Jaguar is a high-performance ab initio package used for both gas and solution phase simulations, with particular strength in treating metal containing systems, like those studied here. Jaguar is an extremely fast quantum mechanics package, and because of the large size of the complexes studied here, it was chosen for the molecular optimization stage.

For each compound a frequency calculation was carried out, verifying that the optimized molecular structure obtained corresponds to an energy minimum, thus only positive frequencies were expected. The exchange-correlation functional B3LYP is a hybrid functional which includes three terms for the exchange: a Hartree-Fock exact exchange, a Slater local exchange, and a Becke non-local exchange, and two terms for the correlation: a local correlation provided by Vosko, Wilk, and Nusair (VWN) and a non-local correlation given by Lee, Yang, and Parr (LYP) [17]. An effective core potential LACVP was used to describe the ruthenium atom, and the basis set used for the lighter atoms (C, N, O, P, H, Cl) was 6-31G with a set of "d" and "p" polarization functions [18].

The TD-DFT (time dependent density functional theory) method [12–14] was employed to calculate the electronic absorption spectra of the complexes in the gas phase, previously optimized, at the B3LYP/LANL2DZ-6-31++G(d) level of calculation using GAUSSIAN03 Rev. E.01 [19]. LANL2DZ is an effective core potential used for the ruthenium atom. The ++ sign represents s and p diffuse functions.

TD-DFT is a quantum mechanic method used in chemistry to investigate the properties of a molecular system in an excited state. The method is based on the knew Runge–Gross theorem [20], which corresponds to the time-dependent analog of the Hohenberg–Kohn theorem [21]. Therefore, it is an extension of the DFT theory where variable time is included as a perturbation. TD-DFT has been successful in the calculation of excited states of isolated chemical systems [22]. In this work 100 singlet excited states was calculated as vertical transitions for all the complexes **1**, **2**,

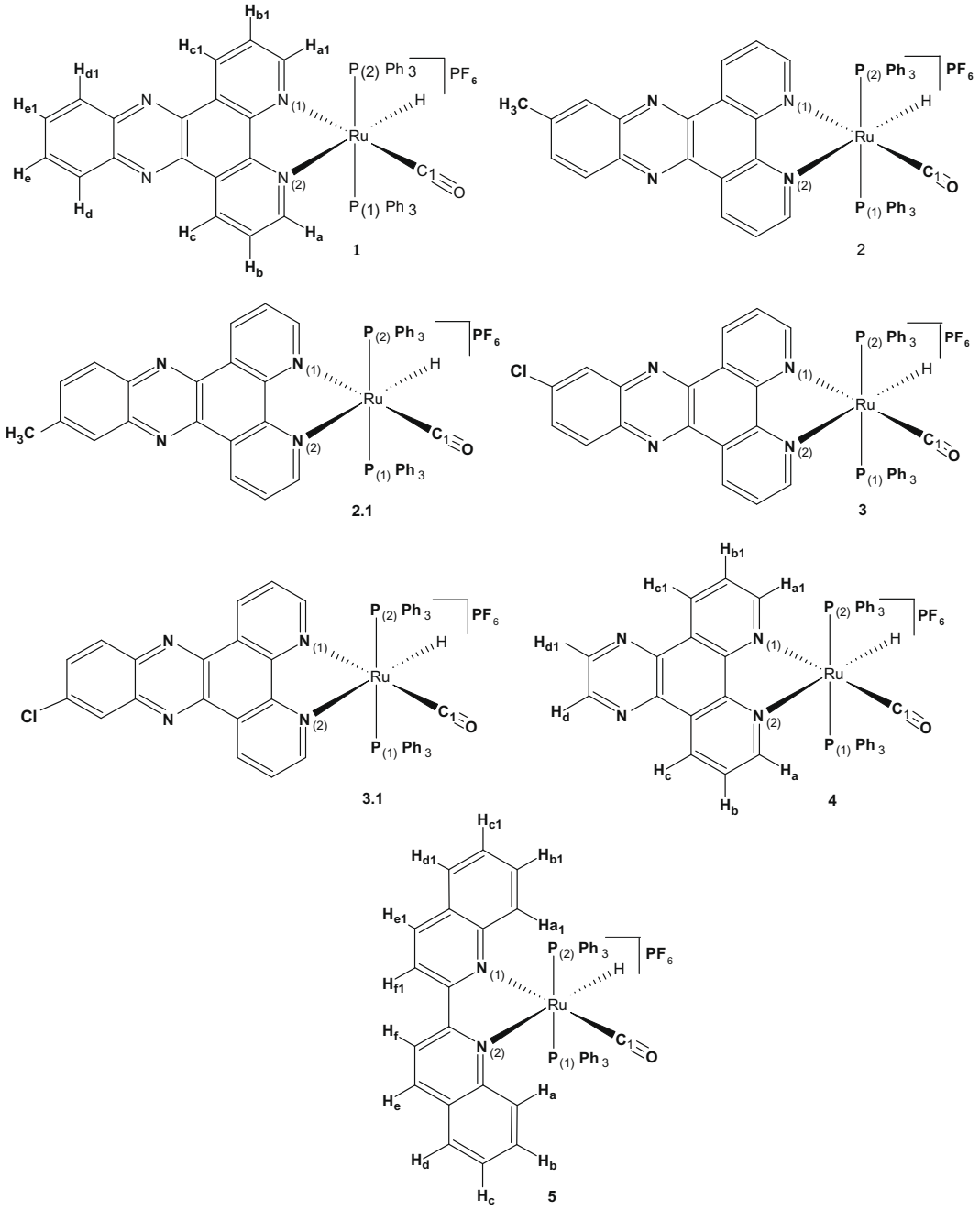

Fig. 1. Molecular structure of the $[RuH(CO)(N\text{-}N)(PPh_3)_2]^+$ complexes with N-N = dppz **(1)**, dppz-CH_3 **(2)**, dppz-Cl **(3)**, ppl **(4)**, biq **(5)**; **2.1** and **3.1** are the isomers of the corresponding complexes.

2.1, **3, 3.1**, **4** and **5**. Due to the size of the complexes, and in order to determine the effect of the solvent on the absorption spectrum, the latter was only calculated for complex **1** in the solution phase (dichloromethane solvent).

A natural bond orbital (NBO) analysis was also made for all the complexes using the NBO 5.0 package [23]. Natural bond orbitals are orbitals localized on one or two atomic centers, that describe molecular bonding in a manner similar to a Lewis electron pair structure, and they correspond to an orthonormal set of localized orbitals of maximum occupancy. NBO analysis provides the contribution of atomic orbitals (s, p, d) to the NBO σ and π hybrid orbitals for bonded atom pairs. In this scheme, three NBO hybrid orbitals are defined, bonding orbital (BD), lone pair (LP), and core (CR), which were analyzed on the atoms directly bonded to or presenting some kind of interaction with the ruthenium atom.

All the complexes were considered in their cationic form, and present a singlet spin multiplicity. The ruthenium atom presents an oxidation state of +2.

4. Results and discussion

4.1. Spectroscopic characterization of the complexes of the series [RuH(CO)(dppz-R)(PPh$_3$)$_2$]PF$_6$ with R = H, Cl, CH$_3$

The ^{31}P NMR spectrum of the $[RuH(CO)(dppz)(PPh_3)_2]PF_6$ complex shows a singlet at 46.5 ppm indicating that the triphenylphosphine ligands are located in a *trans* position in the structure of the complex. The ^2J ^{31}P–^1H couplings are weak, but sufficiently strong to be seen. The signals of phosphorus at −132.4, −138.3, −144.1

and −150 ppm indicate the presence of the hexafluorophosphate counterion.

The ^{1}H NMR spectrum of the [RuH(CO)(dppz)(PPh$_3$)$_2$]PF$_6$ complex (Fig. 2) shows clearly the presence of the aromatic protons of the polypyridine ligand in addition to a set of signals corresponding to the triphenylphosphine ligand. The protons adjacent to the carbonyl group are the most deshielded due to the paramagnetic effect provided by this group. Proton H$_c$ is recorded at very low field because it is also highly deshielded due to the anisotropic effect provided by the nitrogen atom of the pyrazine ring,

The signal is a doublet due to the magnetic *ortho* coupling with H$_b$ ($^3J_{cb}$ = 5.1 Hz). H$_b$ appears as a doublet of doublets by coupling with H$_c$ ($^3J_{bc}$ = 5.1 Hz). H$_a$ and H$_{a1}$ are both recorded as doublets because of their orthocoupling with H$_b$ and H$_{b1}$, respectively ($^3J_{ab}$ = 8.9 Hz), ($^3J_{a1b1}$ = 8.9 Hz). The corresponding signals of H$_d$ + H$_{d1}$:H$_e$ + H$_{e1}$ are multiplets. The signal of H$_{b1}$ overlaps the signals of the protons of the phenyl group, and this is supported by bidimensional NMR (*vide infra*). The signal at high field (−10.9 ppm) indicates the presence of the hydride coordinated with the metal. The shift of the signal is due to the shielding effect of the metal and to the negative charge of the hydrogen atom. The signal is a triplet due to coupling with the two *trans* equivalent phosphorus atoms (J_{HP} = 20.4 Hz).

The ^{31}P NMR spectrum shows a singlet at 46.5 ppm indicating that the triphenylphosphine ligands are located in a *trans* position in the structure of the complex. The ^2J ^{31}P–^{1}H couplings are weak to be observed. The signals of phosphorus at −132.4, −138.3, −144.1 and −150 ppm indicate the presence of the hexafluorophosphate counterion.

The unequivocal proton NMR assignments were made by concerted analysis of 1D ^{1}H, 1D ^{13}C, 2D-ge ^{1}H ^{1}H COSY, 2D ^{1}H ^{13}C HSQC-ed, and 2D ^{1}H ^{13}C HMBC spectra (*vide infra*), which also support the presence of two isomers.

The bidimensional H–H-COSY-NMR spectral analysis of the [RuH(CO)(dppz)(PPh$_3$)$_2$]PF$_6$ complex (see Fig. 3) gives strong support to the assignment made by ^{1}H NMR.

In order to completely characterize the structure of the complexes, a determination of the ^{13}C–^{1}H correlations by HSQC (heteronuclear single quantum correlation) was made (see Fig. S1). This made it possible to know the scalar coupling to one bond between the protons and the heteronucleus of ^{13}C. Finally, using HMBC (heteronuclear multiple bond correlation) experiments, it was possible to obtain the connectivity to two and three bonds, giving strong support to the interpretation of the H–H and H–C correlations for the complexes studied. The HMBC spectrum (Fig. S2) shows a selection of signals which confirms the preliminary assignment carried out for the ^{1}H one-dimensional spectrum. It is clearly seen that the signal for the C$_{14}$–H$_{b1}$ coupling again confirms that the H$_{b1}$ proton is overlapped by the signals of the triphenylphosphine. Both experiments provide enough information to have the complete signal assignment as can be seen in the ^{13}C NMR spectrum (Fig. 4).

The ^{1}H NMR spectrum of the [RuH(CO)(dppz-Cl)(PPh$_3$)$_2$]PF$_6$ complex shows (see Section 2) that H$_d$ is the most unshielded proton because of the presence of a neighbouring chlorine atom. This proton appears as a singlet signal due the absence of coupling with other neighbouring protons. The hydride signal appears at high field (−11 ppm). The ^{31}P NMR spectrum shows a signal at 46.4 ppm, which confirm the *trans* position of the triphenylphosphine ligands. The ^{1}H and ^{31}P NMR spectra of the complexes containing the dppz-CH$_3$ (**2**) y ppl (**4**) ligands are similar to those of the complex analyzed above.

The double pattern of signals seen in the ^{13}C NMR spectra for the complexes with R = CH$_3$ (**2**) and Cl (**3**) suggest that two isomers can be obtained (see Fig. 5), and this is supported by the 2D NMR spectra.

4.2. FT-IR analysis of the complexes of type [RuH(CO)(N-N)(PR$_3$)$_2$]PF$_6$

Complexes of type RuH(CO)(dppz-R)(PPh$_3$)$_2$]PF$_6$ display strong C═O bands between 1937 and 1934 cm^{-1}. The presence of PF_6^- is revealed by the intense bands registered between 838 and 840 cm^{-1}. Stretching vibrations for C═C and C═N are observed in the 1435–1480 cm^{-1} range. The bands for the Ru–H bond are displayed at 2014 and 2009 cm^{-1}, respectively, for the systems with R = CH$_3$ and R = Cl. For the complex with the dppz ligand this particular band is not seen as in others.

The inclusion of an electron-donor substituent such as a methyl in the polypyridine ligand (dppz), produces a decrease of about 3 cm^{-1} in the vibration frequency of the CO bond. This is the result of the net effect of this substituent, which provides electron den-

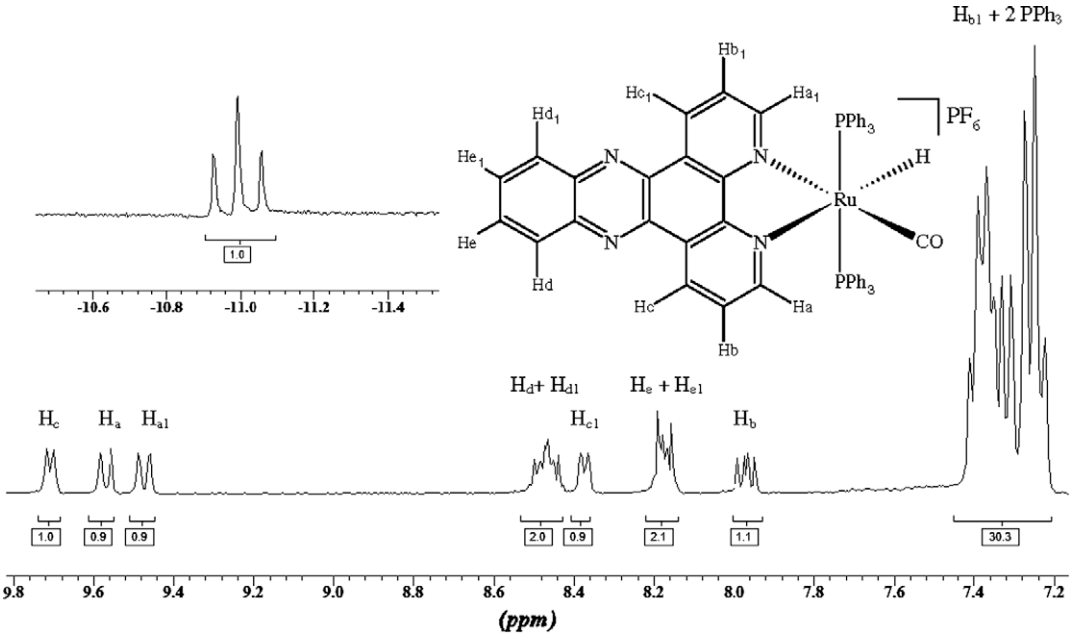

Fig. 2. ^{1}H NMR spectrum of the [RuH(CO)(dppz)(PPh$_3$)$_2$]PF$_6$ complex.

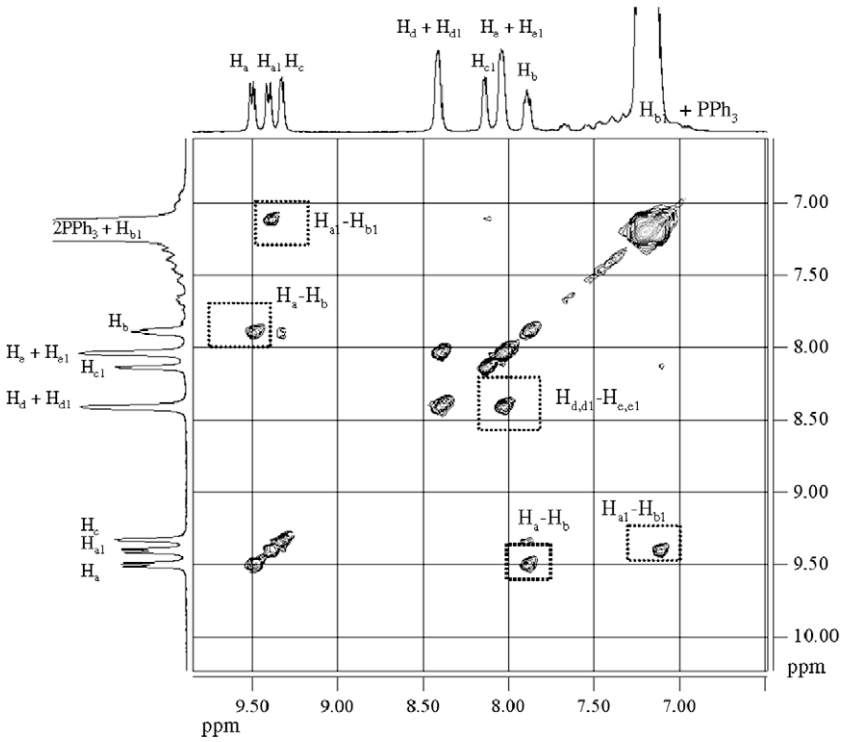

Fig. 3. 2D-H–H COSY spectrum of the[RuH(CO)(dppz)(PPh_3)$_2$]PF_6 complex in $CDCl_3$.

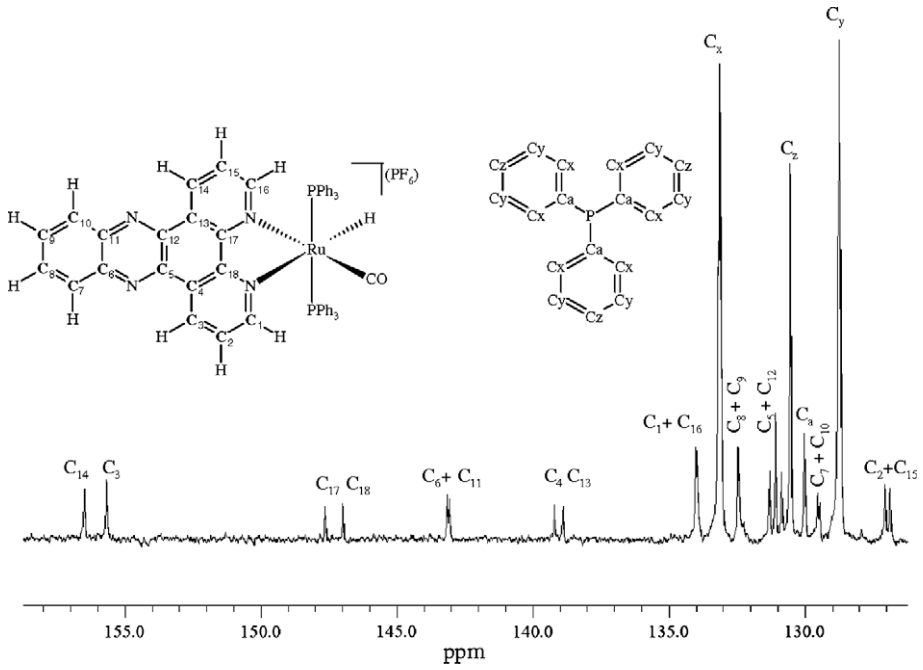

Fig. 4. ^{13}C NMR of the [RuH(CO)(dppz)(PPh_3)$_2$]PF_6 complex in $CDCl_3$.

sity to the metal and this in turn delivers electron density via back-bonding to the anti-bonding orbitals of the CO. This decreases the bond order of CO, thus decreasing the vibration energy of the CO bond.

On the other hand, the inclusion of an electron-acceptor substituent such as chlorine in the dppz ligand should produce a reverse effect, decreasing the electron density on the metal, and therefore increasing the bond order of the CO bond and increasing the vibration frequency. However, this expected behaviour is not seen since the observed vibration frequency was 1934.3 cm^{-1}, which is rather similar to that seen when the substituent is an electron-donor. This anomalous behaviour may be the result of electron delocalization, that is, a resonance effect involving a chlorine atom with the aromatic system of the dppz ligand. This interpretation is supported by theoretically determined charge values. These values indicate that there is no net negative charge on the chlorine atom. Actually, calculations performed at the B3LYP/LACVP(d,p) level provided positive values on the chlorine atom (0.04) in compound **3**.

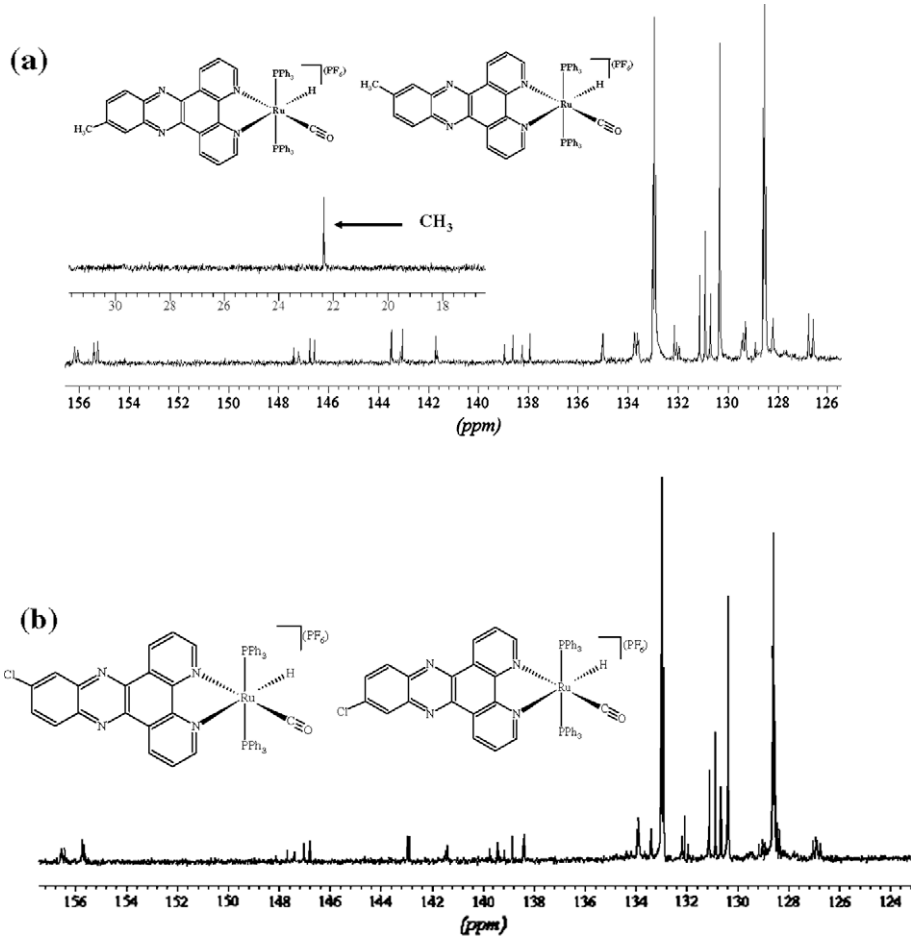

Fig. 5. ^{13}C NMR spectrum of the $[RuH(CO)(dppz\text{-}R)(PPh_3)_2]PF_6$ complex (a) R = CH_3 and (b) R = Cl in $CDCl_3$.

Considering the same electronic effect shown before, the CO vibration frequencies in the complexes with the biq and ppl ligands are 1944 cm^{-1} and 1947 cm^{-1}, respectively, so it can be said that these ligands behave as acceptors with respect to the dppz-R series. In fact, by reducing the electron density on the metal the carbonyl ligand it will receive the electron density via $d\pi \rightarrow \pi^*$ interaction, which would increase the bond order, in turn increasing the vibration frequency of the CO bond.

Besides, we can also see that inclusion in the structure of a phosphine such as methydiphenylphosphine, which is more basic than triphenylphosphine, causes an increase in the vibration frequency of the carbonyl bond from 1937 cm^{-1} to 1942 cm^{-1}, indicating that further donation of sigma electron density from the phosphine to the metal has taken place, that is, the metal provides back-donation of electron density mainly to the d orbitals of phosphorus and not to the orbitals of the Ru–CO bond. Consequently, the bond order of CO increases and the vibration frequency increases by 5 cm^{-1} as observed in the IR spectrum. Vibration frequency values are summarized in Table 1.

4.3. Optimized molecular structures

We studied five complexes of the $[RuH(CO)(N\text{-}N)(PPh_3)_2]^+$ series in their ground state and two diastereomers of the substituted complexes, **2.1** and **3.1**. The results obtained for the optimized molecular structures are shown in Fig. 6 and the more representa-

Table 1
Absorption frequencies for the complexes $[RuH(CO)(N\text{-}N)(PR_3)_2][PF_6]$.

Complex	Absorption frequency IR (cm^{-1}) KBr				
	ν_{Ru-H}	$\nu_{C\equiv O}$	$\nu_{C=C,\ C=N}$	$\nu_{PF_6^-}$	ν_{C-Cl}
$RuHCl(CO)(PPh_3)_3$	2013 (m)	1922 (vs)			
$RuHCl(CO)(PPh_2Me)_3$	No obs	1926 (vs)			
$[RuH(CO)(dppz)(PPh_3)_2)]PF_6$	No obs	1937 (vs)	1435–1480 (m)	838 (vs)	
$[RuH(CO)(dppz\text{-}Cl)(PPh_3)_2]PF_6$	2009 (m)	1934 (vs)	1432–1486 (m)	838 (vs)	1091 (m)
$[RuH(CO)(dppz\text{-}CH_3)(PPh_3)_2]PF_6$	2014 (m)	1934 (vs)	1434–1481 (m)	840 (vs)	
$[RuH(CO)(2,2\text{-biqui})(PPh_3)_2]PF_6$	No obs	1944 (vs)	1433–1509 (m)	839 (vs)	
$[RuHCO(ppl)(PPh_3)_2]PF_6$	No obs	1947 (vs)	1434–1481 (m)	836 (vs)	
$[RuH(CO)(dppz)(PPh_2Me)_2]PF_6$	No obs	1942 (vs)	1419–1490 (m)	838 (vs)	

m: medium; vs: very strong.

Table 2
Bond lengths (Å) and bond angles (°) more relevants for the complexes $[RuH(CO)(N\text{-}N)(PPh_3)_2]^+$ with N-N = dppz **(1)**, dppz-CH_3 **(2)**, dppz-Cl **(3)**, ppl **(4)**, biq **(5)** calculated at the B3LYP/LACVP(d,p) level. **2.1** and **3.1** corresponds to the isomers of the respective complexes.

Bond length[a]	1	2	2.1	3	3.1	4	5
Ru-C_1	1.864	1.866	1.865	1.864	1.864	1.866	1.858
Ru–H	1.601	1.601	1.588	1.598	1.604	1.597	1.577
Ru–P_1	2.463	2.429	2.445	2.456	2.445	2.460	2.453
Ru–P_2	2.428	2.465	2.452	2.441	2.443	2.424	2.466
Ru–N_1	2.177	2.184	2.181	2.169	2.173	2.184	2.244
Ru–N_2	2.235	2.243	2.251	2.264	2.242	2.241	2.319
C_1–O	1.157	1.159	1.159	1.161	1.161	1.159	1.161
Bond angle[a]	**1[a]**	**2**	**2.1**	**3**	**3.1**	**4**	**5**
$<P_1RuP_2$	172.73	170.33	169.42	174.19	171.16	167.21	166.41
$<N_1RuN_2$	75.66	75.57	75.58	75.45	75.80	75.51	74.27
$<HRuC_1$	88.82	89.50	86.86	87.16	89.66	89.84	84.43
$<N_1RuC_1$	177.03	175.38	178.77	178.18	177.92	175.31	179.43
$<N_2RuH$	169.76	170.64	169.63	166.64	168.21	170.26	169.27
$<N_1RuH$	94.13	95.09	94.08	91.18	92.40	94.76	95.11
$<N_2RuC_1$	101.36	99.82	103.45	106.19	102.12	99.86	106.16

[a] For atom numeration see Fig. 1.

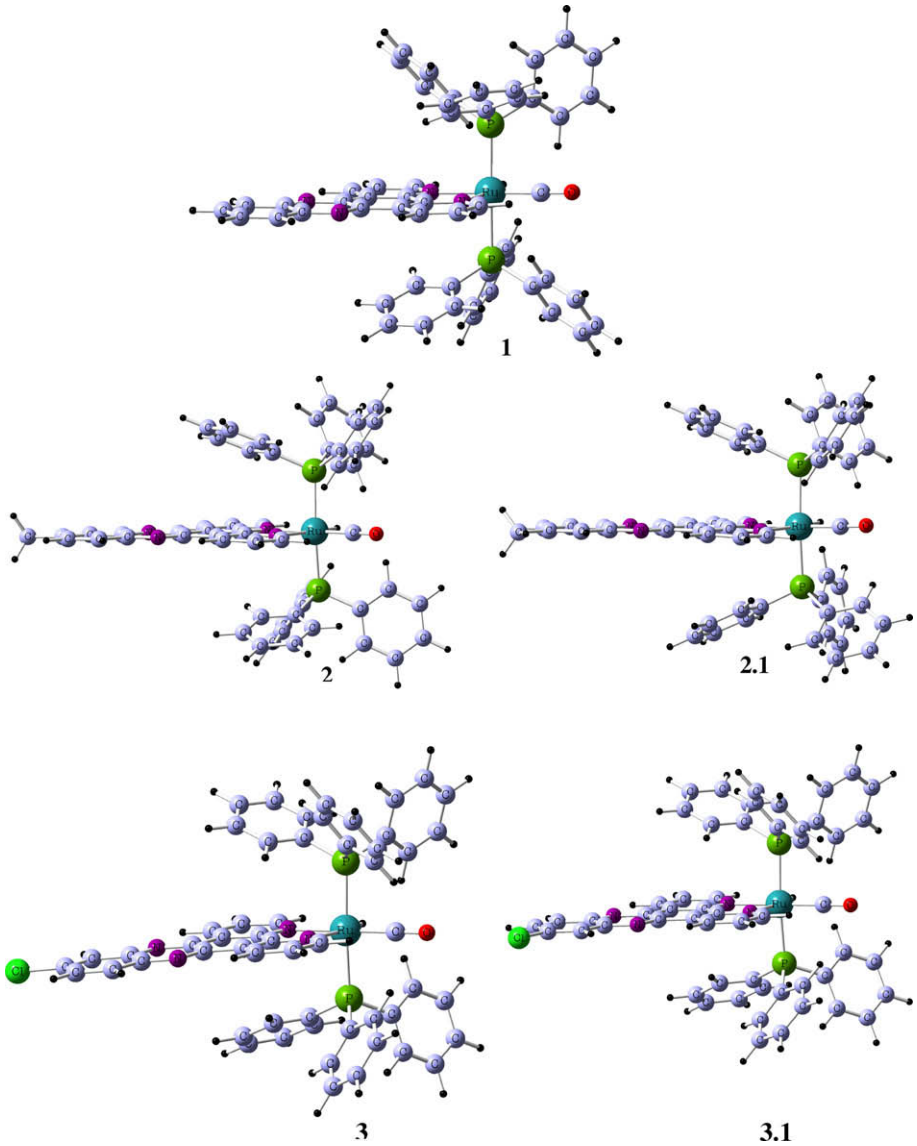

Fig. 6. Optimized molecular structures of the $[RuH(CO)(N\text{-}N)(PPh_3)_2]^+$ complexes with N-N = dppz (**1**), dppz-CH_3 (**2**), dppz-Cl (**3**), ppl (**4**), biq (**5**); **2.1** and **3.1** are the isomers of the corresponding complexes, calculated in the gas phase at the B3LYP/LACVP(d,p) level.

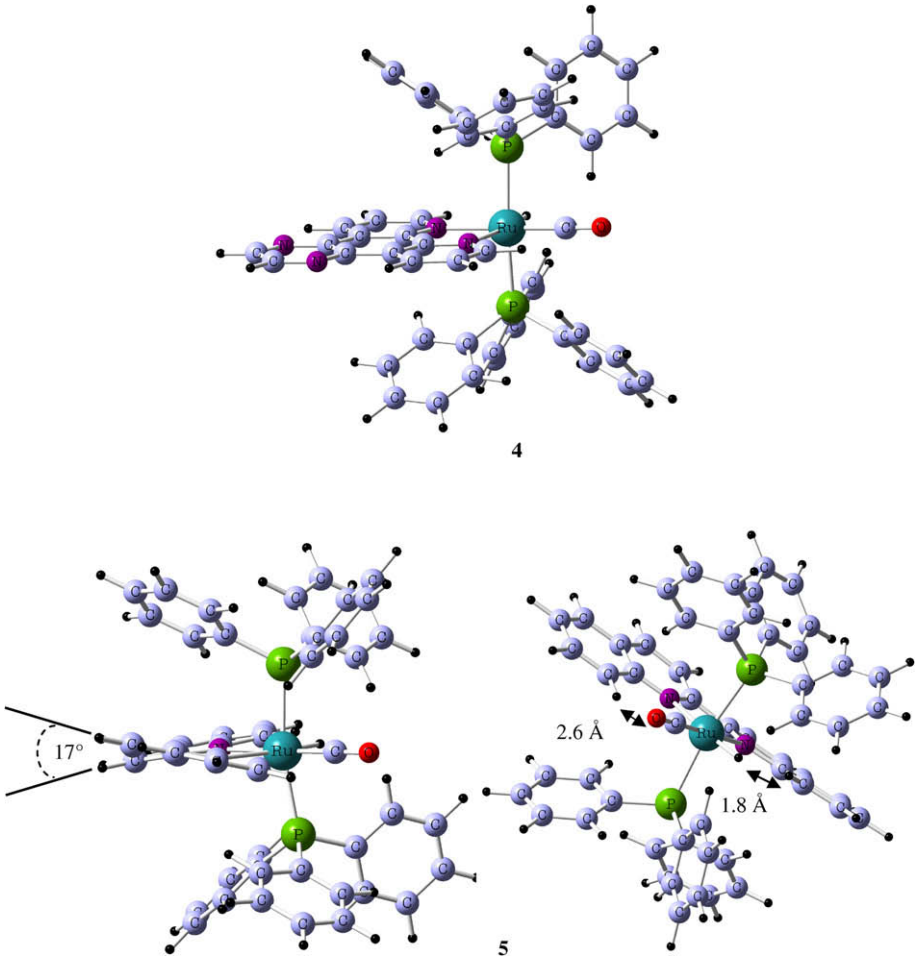

Fig. 6 (*continued*)

tive bond lengths and bond angles of the compounds are presented in Table 2.

The optimized structure of **1** shows a point group C1 distorted octahedral structure with respect to the ligands. It is seen that the triphenylphosphine ligands (PPh_3) are located in a *trans* position, while the polypyridine ligand adopts a *trans* position relative to the carbon monoxide and hydride ligands. In complexes **2** and **3**, the polypyridine ligands dppz-Cl and dppz-CH_3 present the same planarity as the isolated ligands before coordinating with Ru, retaining their aromatic character. The same planarity trend is found with the ppl ligand in **4**, however, in **5** the 2,2′-biquinoline ligand is distorted out of the plane at an angle of 17°. The presence of a single bond connecting both quinolines facilitates rotation around this bond, and it is responsible for the distortion. Optimized geometries show that the Ru–N_1 and Ru–N_2 bonds are different and therefore the structure of the polypyridine ligand is not symmetric. A similar behaviour is seen for the Ru–P_1 and Ru–P_2 bonds. Optimized bond lenghts of the complexes with substitution on the polypyridine ligand (**1**–**3**) does not represent an important change. The larger change with respect to the unsubstituted complex **1** occurs for the Ru–P_1 and Ru–P_2 bonds of complex **2**, with values of 0.034 Å and 0.037 Å, respectively.

On the other hand, a change in the dppz ligand by ppl produces a slight change in the bond lengths of the ligands coordinated to ruthenium. However, the change from dppz to biq generates deviations of the bond lengths of 0.038 Å for Ru–P_2 and 0.023 Å for Ru–H. The Ru–N_1 and Ru–N_2 bonds show the largest changes with respect to **1**, increasing by 0.067 Å and 0.076 Å, respectively, indicating that the effect of a change in the polypyridine ligand produces a modification in the π interaction between the metal and the nitrogen atoms, which can be explained by the size and aromatic character of this ligand.

Table 2 shows that the Ru–C(CO) and C–O (C≡O) bond lengths do not undergo important changes due to the kind of the polypyridine ligand, and only a slight decrease of ∼0.01 Å is seen for biq. In relation to the bond angles associated with the metal atom, the calculations show that these parameters present slight changes. In particular, a reduction of 1° is seen in the chelation angle (N_1RuN_2) of the polypyridine ligand 2,2′-biquinoline, an effect that can be attributed to the presence of a single bond between the two quinolines, favouring rotation around this bond.

4.4. Hybrid orbital and molecular orbital description

Results corresponding to the hybrid orbitals obtained from the NBO analysis of all the compounds of the $[RuH(CO)(N\text{-}N)(PPh_3)_2]^+$ set are shown in terms of atomic composition in Table S1. For all the complexes we found that the nitrogen atoms N_1 and N_2 belonging to the polypyridine ligand do not show covalent bonding with ruthenium. However, the optimized structures (Section 4.3) gave an atomic distance for both Ru–N_1 (2.17–2.18 Å) and Ru–N_2 (2.23–2.32 Å) close to the standard value for a Ru–N bond length [24–27]. This fact can be explained by the donor acceptor energies $E(2)$ calculated with the NBO 5.0 package [23]. $E(2)$ values account for the degree of delocalization of the electronic density

produced between one NBO orbital acting as a donor fragment, and another NBO orbital acting as an acceptor fragment.

Based on the $E(2)$ values, for all the complexes interactions of the lone pair $N_2 \rightarrow \sigma^*$ Ru–H type (47–58 kcal/mol) and lone pair $N_1 \rightarrow \sigma^*$ Ru–C_1 type (75–83 kcal/mol), where σ^* represents the anti-bonding orbital, were found, indicating that a charge transfer occurs. As it can be seen in Fig. 6, the Ru–H bond is colinear with N_2, and the Ru–C_1 bond is colinear with N_1, and this would account for the existence of such interactions. These results suggest a decrease in the strength of the interaction between N_1 and N_2 and Ru, leading to noncovalent bonding.

Table S1 shows that the interactions between the phosphorous atoms (P_1, P_2) of the triphenylphosphines and the ruthenium atom does not follow the same behaviour for all the complexes. For **1**, **2.1** and **4**, a covalent bonding is found for the Ru–P_2 interaction, but a charge transfer of the lone pair $P_1 \rightarrow \sigma^*$ Ru–P_2 type (120–141 kcal/mol) was obtained. An opposite behaviour is found for complexes **2**, **3**, **3.1** and **5**, the covalent bonding is found for Ru–P_1 and the donor acceptor interaction is associated with the lone pair $P_2 \rightarrow \sigma^*$ Ru–P_1 (118–144 kcal/mol). Table S1 shows that all the complexes present the phosphorus atom in the covalent bonding with a nearly sp^3 hybridization, which can account for the tetrahedral environment around the atom in the tetraphenylphosphine ligand. NBO analysis allowed knowing the nature of the coordination between ruthenium and the atoms of the ligands directly interacting with it. This methodology also gave a better understanding of the optimized molecular structures.

Analysis of the frontier molecular orbitals, HOMO (highest occupied molecular orbital), and LUMO (lowest unoccupied molecular orbital) in organometallic compounds like those studied here is useful for understanding the charge transfer that they undergo.

HOMO and LUMO surfaces are shown in Fig. 7, and the composition of these molecular orbitals in terms of the more relevant atomic fragments are given in Table S2. Fig. 7a shows that HOMOs are mainly localized on the ruthenium atom (44–51%), with a contribution of d_{xy} and d_{yz} atomic orbitals. These molecular orbitals also have an important contribution from the triphenylphosphine ligands of 21–26% each. On the other hand, LUMOs (Fig. 7b) are basically located in the polypyridine ligand (93–98%) in atomic orbitals p_y.

Our results suggest that an electron oxidation can occur on ruthenium and on PPh_3, and that an electron reduction can occur on the polypyridine ligand. It means that the complexes studied can present a charge transfer at the intramolecular level from the oxidation sites (Ru, PPh_3) to the reduction sites (dppz, ppl, biq).

4.5. Experimental and theoretical electronic absorption spectra

UV–Vis electronic absorption spectra of all the complexes were measured in dichloromethane. Fig. 8 shows the electronic spectra of complexes **1**, **2** and **3**, which present a change of substitution in the polypyridine ligand. It is seen that these complexes present three absorption bands, one of them of higher intensity and lower wavelength occurs at 232 nm with a value of $\varepsilon = 2.5 \times 10^4$–$4.0 \times 10^4\ cm^{-1}\ M^{-1}$ (Table S3), depending on the complex, which can be associated with electronic transitions of the $\pi \rightarrow \pi^*$ type. A second band of similar ε value appearing at ~280 nm, and a third band of much lower intensity in the 360–380 nm region. The presence of an electron-donor substituent in the polypyridine ligand, such as methyl group (–CH_3) **2**, produces a bathocromic shift of this band with respect to the unsubstituted form **1** (360 nm) in an amount of 12 nm (372 nm). The substituent (–Cl) in **3** also produces a similar bathocromic shift, but a somewhat greater red shift of 24 nm (384 nm) with respect to the unsubstituted compound **1**. Therefore, of the three bands seen, the absorption band of higher wavelength presents a greater change with respect to substitution

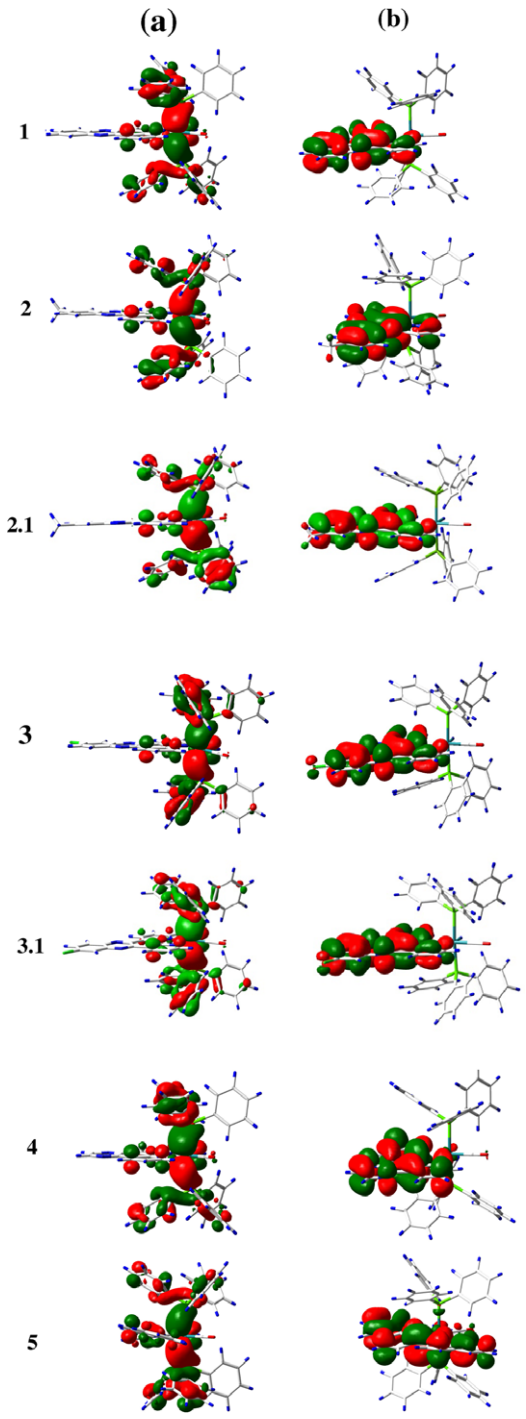

Fig. 7. Molecular surfaces of the (a) HOMO and (b) LUMO frontier molecular orbitals for the set of $[RuH(CO)(N\text{-}N)(PPh_3)_2]^+$ complexes calculated at the B3LYP/LANL2DZ-6-31++G(d) level.

in the polypyridine ligand. It suggests that the –CH_3 and –Cl substituents have an effect on the outermost electrons of the compounds able to produce red shifted absorption bands. Therefore, this kind of substituents can tune the absorption properties of these complexes.

Fig. 9 shows a comparison of the electronic spectra of the compounds that have different polypyridine ligands, **1**, **4** and **5**. A red shift is seen of the lower wavelength band when the polypyridine ligand, which is planar in **1** (360 nm), is replaced by the 2,2′-biquinoline ligand **5** (371 nm). This ligand presents a slight distortion when coordinated with the ruthenium atom because it

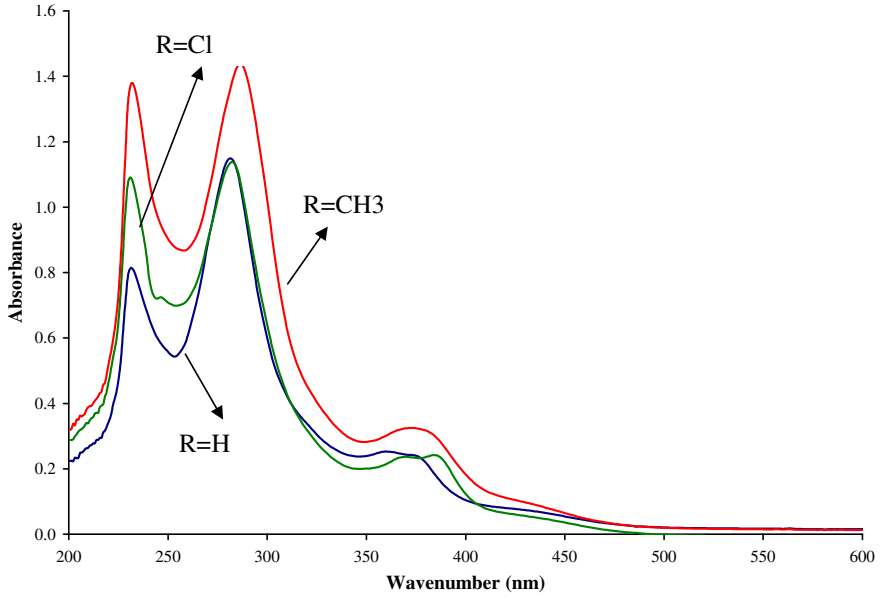

Fig. 8. UV–Vis spectra of the $[RuH(CO)(dppz\text{-}R)(PPh_3)_2]PF_6$ complexes in CH_2Cl_2; R = H **1** blue line, R = CH_3 **2** red line, R = Cl **3** green line. (For interpretation of the references to colour in this figure legend, the reader is referred to the web version of this article.)

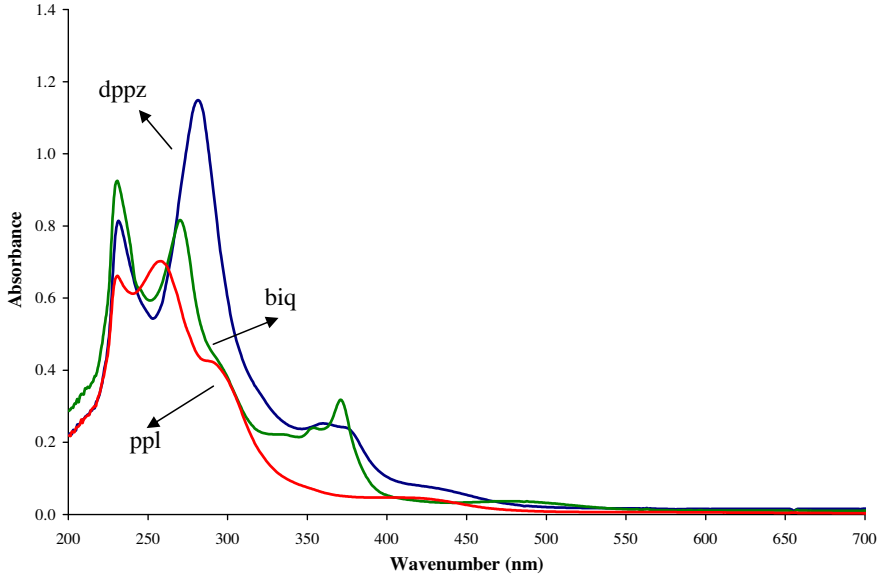

Fig. 9. UV–Vis spectra of the $[RuH(CO)(N\text{-}N)(PPh_3)_2]PF_6$ complexes in CH_2Cl_2 N-N = dppz **1** blue line, N-N = 2,2-biqui **4** green line, N-N = ppl **5** red line. (For interpretation of the references to colour in this figure legend, the reader is referred to the web version of this article.)

presents a single bond between two isoquinolines. A greater red shift is seen for **4,** where the structure of the polypyridine ligand (Fig. 1) suggests a higher electron delocalization.

The full theoretical absorption spectra were obtained from the calculation of the singlet excited states with TD-DFT at the B3LYP/LANL2DZ/6-31++G(d) level in the gas phase. Computation of 100 excited states of all the complexes allowed the interpretation of the experimental spectra in the 230–420 nm range. The excited states assigned to the absorption bands are shown in Table 3 and the full spectra are displayed in Fig. S3.

Previously, we compared for the complex **1** the excited states computed in the gas phase and in the solution phase with dichloromethane as the solvent. The results are included in Supplementary material (Fig. S3). We found that the position of the bands remained constant but their intensity changed. An increased intensity is seen for the theoretical spectrum computed in the solution phase. These results gave theoretical evidence that calculation of the electronic spectra in the gas phase constitutes a very good approximation for these kind of complexes. Therefore, we only computed the spectra of the other complexes in the gas phase.

For the complexes with the dppz ligand (**1**, **2**, **2.1**, **3**, **3.1**), the calculated excited states predict very well the experimental values of the two bands of longer wavelength. In complex **1** the error for the observed band at 360 nm is zero. The maximum error of the theoretical longest wavelength band compared to the experimental one is found for **2**, with 19 nm, and for the second longest wavelength band for **3.1** (9 nm). Anyway, the errors found are negligible.

However, for the shortest wavelength band found for all the complexes at 232 nm, the theoretical calculations predicted it in the range of 263–267 nm. For the assignment of the observed bands to the calculated excited states, both the position and the relative intensity of the former were considered.

Table 3
Experimental (Exp.) and theoretical (Calc.) excitation energies and oscillator strengths (*f*) calculated at the B3LYP/LANL2DZ-6-31++G(d) level for the complexes of the series $[RuH(CO)(N\text{-}N)(PPh_3)_2]^+$ with N-N = dppz (**1**), dppz-CH_3 (**2**, **2.1**), dppz-Cl (**3**, **3.1**), ppl (**4**), biq (**5**).

Excited state	Exp.	Calc.	*f*	Electronic transition	Character[c]
1					
8	3.44[a] (360)[b]	3.44 (360)	0.0458	[d]H-5 → L (−0.27),H-1 → L + 1 (0.38)	MLLCT,MLLCT
48	4.40 (282)	4.32 (287)	0.5294	H-8 → L + 2 (−0.30),H-3 → L + 2 (−0.32)	MLLCT,MLLCT
65	5.34 (232)	4.72 (263)	0.1908	H-1 → L + 3 (0.40), H → L + 7 (0.27)	MLMLCT, MLMLCT
2					
8	3.33 (372)	3.51 (353)	0.0662	H-6 → L (0.32), H-2 → L + 1 (0.22)	MLLCT,MLLCT
44	4.32 (287)	4.23 (293)	0.5664	H-1 → L + 2 (0.29), H-2 → L + 2 (−0.24)	MLLCT, MLLCT
66	5.34 (232)	4.71 (263)	0.2214	H-2 → L + 3 (0.35), H-1 → L + 3 (0.24)	MLMLCT,MLMLCT
2.1					
4	3.33 (372)	3.28 (378)	0.0505	H-2 → L (0.38), H-1 → L (0.49)	LLCT, MLLCT
42	4.32 (287)	4.19 (296)	0.5151	H-2 → L + 2 (0.37), H-8 → L (−0.30)	LLCT,LLCT
63	5.34 (232)	4.64 (267)	0.1616	H-1 → L + 3 (0.41), H-19 → L + 1 (0.30)	MLMLCT, MLLCT
3					
4	3.23 (384)	3.25 (381)	0.0827	H-5 → L (0.24), H-2 → L (0.57)	MLLCT, MLLCT
43	4.40 (282)	4.23 (293)	0.2116	H-8 → L + 2 (0.41), H-7 → L + 2 (−0.26)	LLCT, MLLCT
64	5.34 (232)	4.70 (264)	0.2124	H-1 → L + 3 (0.41), H → L + 3 (−0.31)	MLMLCT, MLMLCT
3.1					
4	3.23 (384)	3.28 (378)	0.0753	H-3 → L (-0.22), H-2 → L (0.60)	MLLCT,LLCT
44	4.40 (282)	4.23 (293)	0.5609	H-1 → L + 2 (0.34), H-7 → L + 2 (0.27)	MLLCT, MLLCT
62	5.34 (232)	4.65 (266)	0.2297	H-1 → L + 3 (0.47), H → L + 3 (−0.31)	MLMLCT, MLMLCT
4					
1	2.94 (422)	2.79 (445)	0.0333	H → L (0.66), H → L + 1 (−0.19)	MLLCT,MLLCT
50	4.35 (285)	4.35 (285)	0.0544	H-6 → L + 3 (0.21), H-3 → L + 3 (0.43)	MLMLCT,MLMLCT
70	4.81 (258)	4.89 (254)	0.3124	H-17 → L + 2 (0.32), H-16 → L + 2 (0.29)	LLCT, MLLCT
89	5.37 (231)	5.26 (236)	0.0247	H-3 → L + 4 (0.29), H-1 → L + 6 (−0.18)	MLMLCT,MLMLCT
5					
13	3.34 (371)	3.64 (341)	0.0710	H-1 → L + 3 (-0.21), H → L + 3 (0.49)	MLMLCT,MLMLCT
24	4.59 (270)	4.19 (297)	0.1301	H-1 → L + 3 (0.37), H → L + 4 (−0.22)	MLMLCT, LMLCT
40	5.37 (231)	4.65 (267)	0.0729	H → L + 5 (0.26), H → L + 7 (−0.21)	MLLCT, MLMLCT

[a] eV.
[b] nm.
[c] MLLCT: metal-ligand to ligand charge transfer; LMLCT: ligand to metal-ligand CT; MLMLCT: metal-ligand to metal-ligand CT; LLCT: ligand to ligand CT.
[d] H: HOMO; L: LUMO.

In the case of the diastereomers, considering only the first observed band where the major change is due to the position of the substituent, complex **2.1** (378 nm) and complex **3** (381 nm) reproduce well the experimental results of 372 nm and 384 nm, respectively. The other observed bands of these complexes present similar values for the diastereomers (**2**, **2.1** and **3**, **3.1**). These results indicate that the position of the substituent, that is *cis* or *trans* to the ligand CO, is more important in excited states localized in the region near 400 nm, and shows the needed to consider all the isomeric structures.

For a better understanding of the observed bands, the corresponding calculated excited states can be interpreted in terms of electronic transitions between occupied and unoccupied molecular orbitals. Table 3 shows the two electronic transitions of largest contribution to the corresponding excited states.

In complex **1**, excited state 8, which reproduces the observed 360 nm band, predicts electronic transitions of the H-5 → L and H-1 → L + 1 type. We found that H-1 is preferentially located on ruthenium (38%) and on the two PPh_3 ligands (58%), and L + 1 is located on the phenanthroline fragment (89%) of the polypiridine ligand (Table S2). The H-5 molecular orbital has a smaller contribution of Ru (2%) and a larger contribution of one PPh_3 ligand (87%), and L is found preferentially on the dppz ligand (98%) (Table S2). These results suggest that the absorption band at 360 nm corresponds to a charge transfer occurring from the metal and the phosphine ligand regions toward the polypyridine ligand, and therefore it can be assigned to a metal-ligand to ligand charge transfer (MLLCT) character. The bands at 282 nm and 232 nm are predicted by the excited states 48 and 65, respectively, and are attributed to MLLCT and MLMLCT (metal-ligand to metal-ligand charge transfer), respectively.

For complexes **2.1** and **3** we found for the red shifted band that the major contribution corresponds to a charge transfer of the MLLCT type, with the H-1 → L and H-2 → L electronic transitions, respectively. However, the charge transfer in both complexes is different. In **2.1** the charge transfer goes from the region of ruthenium (45%) and both phosphine ligands toward the dppz-CH_3 ligand. In **3** the H-2 molecular orbital is located in ruthenium (13%), dppz-Cl, and both phosphine ligands, and the charge transfer occurs completely toward the dppz-Cl ligand (Table S2).

It is seen that the main differences found due to the presence of a substituent on the dppz ligand are in the initial molecular orbital participating in the charge transfer. In complex **1** it corresponds to 38% in Ru and 58% in phosphine ligands, in **2.1** the values are 45% Ru and 49% PPh_3, and in **3** the values are 13% Ru and 24% PPh_3. These results indicate an effect of the properties of the substituents (–CH_3) and (–Cl).

In contrast to complex **1**, the second band of **2.1** and **3** predicted as the excited states 42 and 43, respectively, is associated with the ligand to ligand charge transfer (LLCT), in the region of the dppz ligand. The observed bands at 232 nm for **2.1** and **3** are predicted by the excited states 63 (267 nm) and 64 (264 nm), respectively, and attributed to a charge transfer MLMLCT.

We also studied what happens by changing the polypyridine ligand in the complex: dppz (**1**), ppl (**4**) and biq (**5**). Again, we found a major change in the excited state associated to the higher wavelength band, as expected. The other excited states of these complexes does not present dramatic changes due to the polypyridine ligand.

Table 3 shows that the band in complex **4** at 422 nm is predicted by the calculation as excited state 1 at 445 nm, with an error of 23 nm. The increased wavelength value with respect to the unsubstituted form (**1**) can be attributed to the more extended π current of the molecular structure (Fig. 1).

In complex **5**, the observed band at 371 nm is blue shifted in the calculation to 341 nm (excited state 13), with an error of 30 nm. The excited states for complexes **1** and **4** indicated that the charge transfer is MLLCT. In both cases the main contribution in the arrival molecular orbital of the electronic transition is located on the polypyridine ligand (89% on dppz for **1**, 94% on ppl for **4**). In contrast, in complex **5** the arrival molecular orbital of the transition is centered on ruthenium (31%) and both phosphine ligands (62%), so the charge transfer is MLMLCT.

The results discussed in this section showed the same trend as the experimental data, showing that the TD-DFT methodology and the B3LYP functional were appropriate.

5. Summary

A theoretical and experimental study of the characterization of ruthenium hydride complexes with triphenylphosphine and polypyridine ligands $[RuH(CO)(N\text{-}N)(PPh_3)_2]^+$ with N-N = dppz **1**, dppz-CH_3 **2** (**2.1** isomer), dppz-Cl **3** (**3.1** isomer), ppl **4** and 2,2′-biquinoline **5,** has been made. We studied how a change in the polypyridine ligand (**1**, **4**, **5**) and a change of the substituent in the polypyridine ligand (**1**, **2**, **2.1**, **3**, **3.1**) affect the electronic properties of these complexes. A molecular orbital description of HOMOs and LUMO's showed that all the complexes studied can present an intramolecular charge transfer of the metal (∼50%) – ligand (triphenylphosphine ∼ 43%) to ligand (polypyridine ∼ 93–98%) type).

One hundred of the excited states of each complex were calculated in the gas phase using TD-DFT, and good agreement with the experimental absorption spectra was obtained. The excited states calculated for the seven complexes showed theoretical evidence of the substituent effect on the polypyridine ligand and of ligand effect (dppz, biq, ppl). The theoretical results showed that the properties of these complexes can be tuned easily by introducing substituents into the polypyridine ligand.

Acknowledgements

The authors acknowledge the financial support of FONDECYT under Project 1085135, and the computational time provided by the DICYT-USACH Complementary Support Project. M.Y. thanks CONICYT for a doctoral fellowship and terminal thesis fellowship.

Appendix A. Supplementary material

Supplementary data associated with this article can be found, in the online version, at doi:10.1016/j.jorganchem.2009.07.028.

References

[1] M. Rosales, B. Alvarado, F. Arrieta, C. de la Cruz, A. González, K. Molina, O. Soto, Y. Salazar, Polyhedron 27 (2008) 530.
[2] (a) L. Salvi, A. Salvini, F. Micoli, C. Bianchini, W. Oberhauser, J. Organomet. Chem. 692 (2007) 1442;
(b) D. Di Tommaso, S.A. French, C. Richard, A. Catlow, J. Mol. Struct. (THEOCHEM) 812 (2007) 39.
[3] C. Po Lau, S. Man Ng, G. Jia, Z. Lin, Coord. Chem. Rev. 251 (2007) 2223.
[4] R. Ben Said, B. Tangour, J.C. Barthelat, J. Mol. Struct. (THEOCHEM) 857 (2008) 115.
[5] C. Jun Yue, Y. Liu, R. He, J. Mol. Catal. A: Chem. 259 (2006) 17.
[6] F. Nipa Haque, A.J. Lough, R.H. Morris, Inorg. Chim. Acta 361 (2008) 3149.
[7] P. Buskens, D. Giunta, W. Leitner, Inorg. Chim. Acta 357 (2004) 1969.
[8] J. Bravo, J. Castro, S. García-Fontána, M.C. Rodríguez-Martínez, G. Albertin, S. Antoniutti, A. Manera, J. Organomet. Chem. 692 (2007) 5481.
[9] J.G. Małecki, R. Kruszynski, D. Tabak, J. Kusz, Polyhedron 26 (2007) 5120.
[10] J. Concepción, B. Loeb, Y. Simón-Manso, F. Zuloaga, Polyhedron 19 (2000) 2297.
[11] M. Bortoluzzi, E. Bordignon, G. Paolucci, B. Pitteri, Polyhedron 26 (2007) 4936.
[12] R.E. Stratmann, G.E. Scuseria, M.J.J. Frisch, Chem. Phys. 109 (1998) 8218.
[13] R. Bauernschmitt, R. Ahlrichs, Chem. Phys. Lett. 256 (1996) 454.
[14] M.E. Casida, C. Jamorski, K.C. Casida, D.R. Salahub, J. Chem. Phys. 108 (1998) 4439.
[15] (a) A.J. Gordon, R.A. Ford, The Chemist's Companion: A Handbook of Practical Data, Techniques and References, John Wiley and Sons, 1972;
(b) R. López, S.A. Moya, C. Zúñiga, M. Yánez, J.C. Bayon, P. Aguirre, Appl. Organometal. Chem. 20 (2006) 315.
[16] Jaguar, Version 6.0, Schrödinger, LLC, New York, NY, 2005.
[17] (a) C. Lee, W. Yang, R.G. Parr, Phys. Rev. B 37 (1988) 785;
(b) B. Miehlich, A. Savin, H. Stoll, H. Preuss, Chem. Phys. Lett. 157 (1989) 200;
(c) A.D. Becke, J. Chem. Phys. 98 (1993) 5648.
[18] P.J. Hay, W.R. Wadt, J. Chem. Phys. 82 (1985) 299.
[19] M.J. Frisch, G.W. Trucks, H.B. Schlegel, G.E. Scuseria, M.A. Robb, J.R. Cheeseman, J.A. Montgomery Jr., T. Vreven, K.N. Kudin, J.C. Burant, J.M. Millam, S.S. Iyengar, J. Tomasi, V. Barone, B. Mennucci, M. Cossi, G. Scalmani, N. Rega, G.A. Petersson, H. Nakatsuji, M. Hada, M. Ehara, K. Toyota, R. Fukuda, J. Hasegawa, M. Ishida, T. Nakajima, Y. Honda, O. Kitao, H. Nakai, M. Klene, X. Li, J.E. Knox, H.P. Hratchian, J.B. Cross, V. Bakken, C. Adamo, J. Jaramillo, R. Gomperts, R.E. Stratmann, O. Yazyev, A.J. Austin, R. Cammi, C. Pomelli, J.W. Ochterski, P.Y. Ayala, K. Morokuma, G.A. Voth, P. Salvador, J.J. Dannenberg, V.G. Zakrzewski, S. Dapprich, A.D. Daniels, M.C. Strain, O. Farkas, D.K. Malick, A.D. Rabuck, K. Raghavachari, J.B. Foresman, J.V. Ortiz, Q. Cui, A.G. Baboul, S. Clifford, J. Cioslowski, B.B. Stefanov, G. Liu, A. Liashenko, P. Piskorz, I. Komaromi, R.L. Martin, D.J. Fox, T. Keith, M.A. Al-Laham, C.Y. Peng, A. Nanayakkara, M. Challacombe, P.M.W. Gill, B. Johnson, W. Chen, M.W. Wong, C. Gonzalez, J.A. Pople, GAUSSIAN 03, Revision E.01, GAUSSIAN, Inc., Wallingford, CT, 2005.
[20] E. Runge, E.K.U. Gross, Phys. Rev. Lett. 52 (1984) 997.
[21] P. Hohenberg, W. Kohn, Phys. Rev. B864 (1964) 136.
[22] (a) M.R. Silva-Junior, M. Schreiber, S.P.A. Sauer, W. Thiel, J. Chem. Phys. 129 (2008) 104103;
(b) M. Palma, G.I. Cárdenas-Jirón, M.I. Menéndez Rodríguez, J. Phys. Chem. A 112 (2008) 13574;
(c) M.F. Charlot, A. Aukauloo, J. Phys. Chem. A 111 (2007) 11661.
[23] NBO 5.0. E.D. Glendening, J.K. Badenhoop, A.E. Reed, J.E. Carpenter, J.A. Bohmann, C.M. Morales, F. Weinhold, Theoretical Chemistry Institute, University of Wisconsin, Madison, WI, 2001.
[24] Y. Yuan, Y. Chen, Y. Wang, Ch. Su, S. Liang, H. Chao, L. Ji, Inorg. Chem. Commun. 11 (2008) 1048.
[25] E. Lebon, I. Dixon, L. Vendier, A. Igau, P. Sutra, Inorg. Chim. Acta 360 (2007) 1235.
[26] D.F. Mullica, J.M. Farmer, J.A. Kautz, S.L. Gipson, Y.F. Belay, M.S. Windmiller, Inorg. Chim. Acta 285 (1999) 318.
[27] J. Bravo, J. Castro, S. García-Fontána, M.C. Rodríguez-Martínez, G. Albertin, S. Antoniutti, A. Manera, J. Organomet. Chem. 692 (2007) 5481.